Creating a neuroprosthesis for active tactile exploration of textures

Joseph E. O'Doherty[a,1,2], Solaiman Shokur[b,c,1,3], Leonel E. Medina[a,4], Mikhail A. Lebedev[d,e,f,g], and Miguel A. L. Nicolelis[a,d,e,h,i,j,k,5]

[a]Department of Biomedical Engineering, Duke University, Durham, NC 27708; [b]Neurorehabilitation Laboratory, Associação Alberto Santos Dumont para Apoio à Pesquisa (AASDAP), São Paulo, Brazil, 05440-000; [c]School of Engineering, Institute of Microengineering, École Polytechnique Fédérale de Lausanne (EPFL), 1016 Lausanne, Switzerland; [d]Department of Neurobiology, Duke University Medical Center, Durham, NC 27710; [e]Duke Center for Neuroengineering, Duke University, Durham, NC 27710; [f]Center for Bioelectric Interfaces of the Institute for Cognitive Neuroscience, National Research University Higher School of Economics, Moscow, Russia 101000; [g]Department of Information and Internet Technologies of Digital Health Institute, I.M. Sechenov First Moscow State Medical University, Moscow, Russia 119146; [h]Department of Neurology, Duke University, Durham, NC 27710; [i]Department of Neurosurgery, Duke University, Durham, NC 27710; [j]Department of Psychology and Neuroscience, Duke University, Durham, NC 27708; and [k]Edmond and Lily Safra International Institute of Neuroscience, Macaíba, Brazil 59280-000

Edited by Giacomo Rizzolatti, University of Parma, Parma, Italy, and approved September 11, 2019 (received for review May 12, 2019)

Intracortical microstimulation (ICMS) of the primary somatosensory cortex (S1) can produce percepts that mimic somatic sensation and, thus, has potential as an approach to sensorize prosthetic limbs. However, it is not known whether ICMS could recreate active texture exploration—the ability to infer information about object texture by using one's fingertips to scan a surface. Here, we show that ICMS of S1 can convey information about the spatial frequencies of invisible virtual gratings through a process of active tactile exploration. Two rhesus monkeys scanned pairs of visually identical screen objects with the fingertip of a hand avatar—controlled first via a joystick and later via a brain–machine interface—to find the object with denser virtual gratings. The gratings consisted of evenly spaced ridges that were signaled through individual ICMS pulses generated whenever the avatar's fingertip crossed a ridge. The monkeys learned to interpret these ICMS patterns, evoked by the interplay of their voluntary movements and the virtual textures of each object, to perform a sensory discrimination task. Discrimination accuracy followed Weber's law of just-noticeable differences (JND) across a range of grating densities; a finding that matches normal cutaneous sensation. Moreover, 1 monkey developed an active scanning strategy where avatar velocity was integrated with the ICMS pulses to interpret the texture information. We propose that this approach could equip upper-limb neuroprostheses with direct access to texture features acquired during active exploration of natural objects.

neuroprosthetics | sensory feedback | brain–machine interface

Sensory neuroprostheses offer the promise of restoring perceptual function to people with impaired sensation (1, 2). In such devices, diminished sensory modalities [e.g., hearing (3), vision (4, 5), or cutaneous touch (6–8)] are reenacted through streams of artificial input to the nervous system, typically using electrical stimulation of nerve fibers in the periphery or neurons in the central nervous system. Restored cutaneous touch, in particular, would be of great benefit for the users of upper-limb prostheses, who place a high priority on the ability to perform functions without the need to constantly engage visual attention (9). This could be achieved through the addition of artificial somatosensory channels to the prosthetic device (1). Such an approach would endow persons suffering from limb loss (10–12), paralysis (1, 13), or somatosensory deficits with the ability to perform active tactile exploration of their physical environment and aid in dexterous object manipulation (14–17).

Previously, we demonstrated that motor and sensory functions could be simultaneously enacted through a bidirectional neuroprosthetic system, called a brain-machine-brain interface (BMBI) (18). In that demonstration, the active exploration enabled by our BMBI-driven neuroprosthesis used a limited and fixed set of intracortical microstimulation (ICMS) temporal patterns to generate artificial sensory inputs that mimicked the sense of flutter vibration. However, it remained unclear whether the same approach could generalize to allow a subject to identify the texture of objects and materials by scanning them with the fingertips.

Haptic exploration of objects involves several stereotypic procedures, such as static contact for temperature sensation, holding for weight, enclosure for gross shape, pressure for hardness, contour following for exact shape, and lateral fingertip motion for texture (19). Here, we developed a neuroprosthetic paradigm to functionally reproduce the sensation of fingertip motion against texture. We hypothesized that ICMS pulses generated by exploratory movements over virtual gratings and delivered to primary somatosensory cortex (S1) would allow discrimination of texture coarseness.

Results

Active Texture Encoding. Two rhesus monkeys (monkey M and monkey N) were chronically implanted with multielectrode cortical

Significance

Sensory neuroprostheses offer the promise of restoring perceptual function to people with impaired sensation. Here, we developed a paradigm using intracortical microstimulation (ICMS) for encoding the sensation of fingertip motion against texture. Monkeys learned to interpret time-varying ICMS patterns, evoked by the interplay of their voluntary movements and specific object textures, and discriminated texture coarseness relying solely on these pulse trains. As such, variations in exploration strategy directly affected the timing of individual stimulation pulses. Crucially, this encoding enabled real-time active exploration of textures. We propose that this approach could equip upper-limb neuroprostheses with functional access to texture features acquired during active exploration of natural objects.

Author contributions: J.E.O., S.S., M.A.L., and M.A.L.N. designed research; J.E.O., L.E.M., M.A.L., and M.A.L.N. performed research; J.E.O., S.S., M.A.L., and M.A.L.N. analyzed data; and J.E.O., S.S., M.A.L., and M.A.L.N. wrote the paper.

The authors declare no competing interest.

This article is a PNAS Direct Submission.

Published under the PNAS license.

[1]J.E.O. and S.S. contributed equally to this work.

[2]Present address: Department of Neuroscience, Neuralink Corp., San Francisco, CA 94110.

[3]Present address: Bertarelli Foundation Chair in Translational Neuroengineering, Center for Neuroprosthetics and Institute of Bioengineering, School of Bioengineering, EPFL, 1202 Geneva, Switzerland.

[4]Present address: Departamento de Ingeniería Informática, Universidad de Santiago de Chile, 9160000 Santiago, Chile.

[5]To whom correspondence may be addressed. Email: nicoleli@neuro.duke.edu.

This article contains supporting information online at www.pnas.org/lookup/suppl/doi:10.1073/pnas.1908008116/-/DCSupplemental.

First published October 7, 2019.

Downloaded at Palestinian Territory, occupied on November 29, 2021

www.manaraa.com

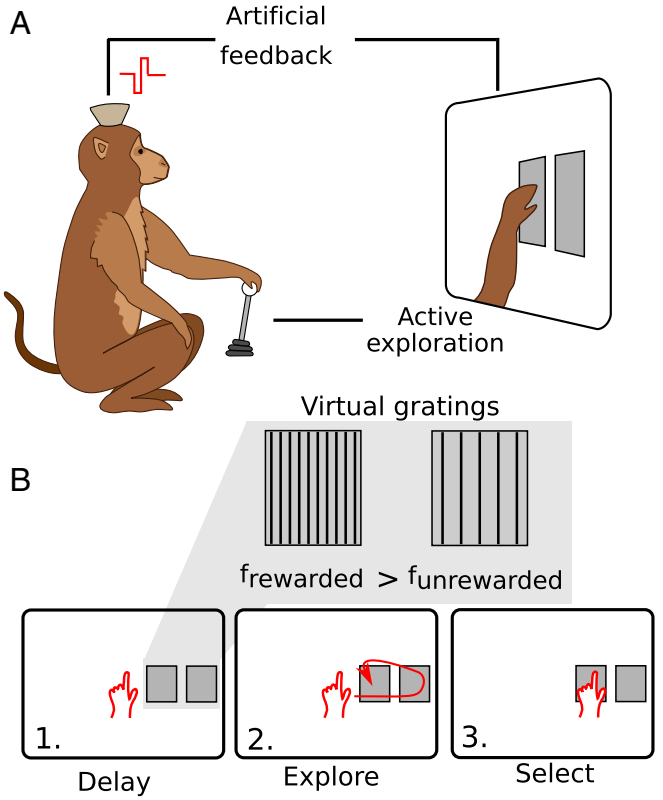

Fig. 1. The artificial texture paradigm. (*A*) A monkey is seated before a display on which an avatar arm and 2 identical objects are projected. Artificial tactile feedback about the virtual gratings associated with each object is delivered to populations of S1 neurons via temporal patterns of ICMS as the monkey actively scans each object. (*B*) Trials commenced with a random delay interval when the monkey held the index finger of the avatar in the center of the screen (1). Next, was the exploration interval (2). Two rectangular objects appeared, and the monkey scanned these objects with the index finger of the avatar hand. Each object had an associated virtual grating of vertical lines, which were invisible to the monkey. A pulse of ICMS was delivered to a pair of electrodes in S1 with each crossing of the avatar index finger over a line in one of the gratings. The trial was completed when the monkey indicated its selection (3) by holding the avatar hand over one of the objects for a hold interval. The reward was delivered if the monkey selected the object with the higher virtual grating frequency (*Inset*); selecting the object with the lower grating frequency ended the trial without reward.

arrays (18) (*SI Appendix*, Fig. S1). These animals explored virtual objects on a computer screen using a realistic upper-limb avatar (*SI Appendix*, Fig. S2), which they operated manually with a joystick (Fig. 1*A*) or using a brain-machine interface (BMI). On each trial, a pair of rectangles appeared either on the left or on the right side of the screen. The rectangles were visually identical, but each was associated with an invisible tactile grating with properties that were randomly chosen for each trial and signaled by charge-balanced ICMS pulses applied to S1 (a region exhibiting left forearm receptive fields for monkey M and left lower-limb receptive fields for monkey N). Each grating consisted of evenly spaced vertical ridges, which were invisible to the monkeys. The spatial frequency of the ridges, f, ranged from 0.5 to 4.0 ridges/cm; an untextured object with no ridges (f = 0 ridges/cm) was also presented on some trials.

The behavioral task required the monkeys to probe the rectangles with the avatar's fingertip, determine which of the 2 had a higher f, and to hold the avatar over that object for the required interval, 2 s in most cases (Fig. 1*B*). The artificial sensation was encoded by delivering a charge-balanced ICMS pulse each time the avatar fingertip crossed a ridge in a grating. Thus, the pulse trains of ICMS delivered on any given trial provided an artificial signal that depended on the interplay between the movements of the avatar and the f of the textures of the explored objects (Movie S1). Movements at a constant velocity across a grating with a given f produced an ICMS pulse train with a constant temporal pulse rate (Fig. 2*A*). Movements at a faster velocity across the same grating produced a pulse train with a correspondingly higher pulse rate (Fig. 2*B*). Irregular movements produced temporally varying ICMS pulse trains (Fig. 2*C*). The objects' adjacent spacing on the screen encouraged the monkeys to shift the avatar from one object to the other and determine which one had a denser grating. The monkeys were permitted to explore the objects in any sequence and enter each object multiple times, to accumulate evidence, before making the selection. Accordingly, the monkeys could select an object on the first pass (Fig. 2 *D* and *E*) or employ several explorations of individual objects (Fig. 2*F*) before making a final selection. Prior to these experiments, these monkeys participated in other studies (18, 20, 21) and became proficient in using the joystick and the hand avatar and making decisions using ICMS pulse trains. The electrodes' placement remained implanted and unchanged throughout all these studies. However, none of the previous experiments employed the particular ICMS encoding rule or the texture scanning paradigm presented in the current study.

Active Texture Discrimination. Both monkeys learned the task rapidly, reaching high-performance levels (71% of correct trials for monkey N, and 73% for monkey M) after 10 daily sessions of training (Fig. 3 *A* and *B*). The average performance was above chance even in the first training session (64% for monkey N and 56% for monkey M). For monkey M, task difficulty was

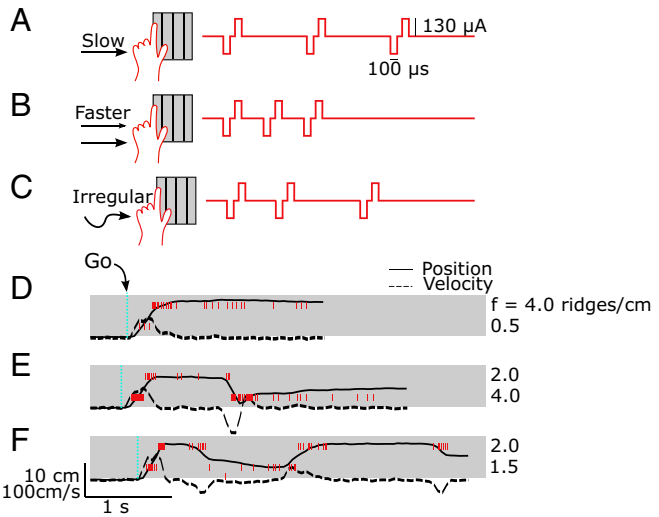

Fig. 2. The precise temporal pattern of ICMS delivered on any trial depended both on the intrinsic spatial frequency of each object's virtual grating as well as the velocity with which the monkey scanned each object. For a grating with a given spatial frequency, slow scanning (*A*) would produce a lower ICMS pulse rate than faster scanning (*B*). (*C*) Irregular scanning of a grating produced irregular ICMS pulse trains. All other features of the pulse train (e.g., current amplitude and pulse width) were fixed. (*D*–*F*) Examples of trials for 3 values of Δf: 3.5 (4.0 vs. 0.5) ridges/cm (*D*), 2.0 (2.0 vs. 4.0) ridges/cm (*E*), and 0.5 (2.0 vs. 1.5) ridges/cm (*F*), respectively. Traces indicate the x-component of the avatar position (solid lines) and velocity (dashed lines). Gray rectangles indicate the position and horizontal dimension of the objects. Red vertical lines indicate single pulses of ICMS. Trials started with a randomized hold-time (200–2,000 ms); a Go cue informed the monkey of the beginning of the exploration interval.

Downloaded at Palestinian Territory, occupied on November 29, 2021
www.manaraa.com

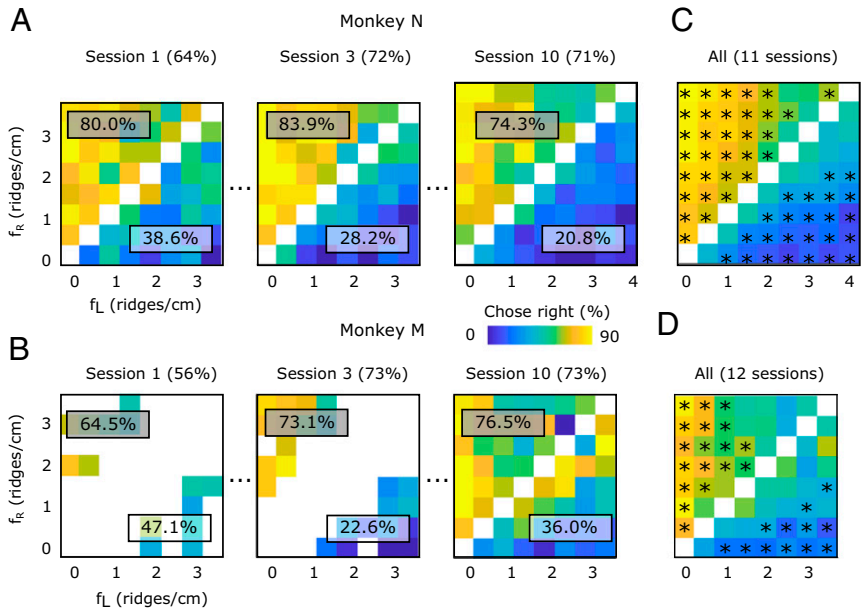

Fig. 3. Monkeys discriminated spatial gratings based on self-generated temporal ICMS. (*A* and *B*) Probability of choosing the right-most object, parameterized by the spatial frequencies of the right object (f_R) and the spatial frequencies of the left object (f_L), for monkey N (*A*) and Monkey M (*B*), for their 1st, 3rd, and 10th sessions. The overall probability of choosing the right-most object considering all trials where $f_R > f_L$ is reported in the gray box in the upper left part of each graph (respectively in the white box in the lower right part for trials where $f_L > f_R$). For each graph, we also report the overall success rate of the session (value shown in parentheses in the title). (*C* and *D*) The performance across all sessions (11 sessions for monkey N, $n = 10{,}412$ trials and 12 for monkey M, $n = 5{,}828$). Asterisks indicate frequency-pair combinations in which discrimination rate was significantly better than chance ($P < 0.05$, 2-sided binomial test). Monkey M was not exposed to gratings with 4.0 ridges/cm.

increased gradually, with a large difference in f introduced early in training, $\Delta f \geq 2$ ridges/cm; $\Delta f < 2$ ridges/cm after 3 sessions and the full range from $f = 0$ to $f = 3.5$ ridges/cm and a minimum $\Delta f = 0.5$ by the end of training. The range for monkey N was $f = 0$ to $f = 3.5$ ridges/cm at the onset of the training and $f = 0$ to $f = 4$ by the end. The minimum difference between textures presented on a trial, Δf, was maintained at 0.5 for all sessions. Fig. 3 *C* and *D* shows the behavioral performance after learning (11 and 12 recording sessions for monkeys M and N, respectively). Both monkeys performed better on individual trials when presented with a pair of objects with larger Δf, as might be expected. However, we observed an additional scaling of discrimination difficulty that depended on the absolute scale of the spatial frequencies of the objects being compared. More specifically, the psychometric functions for both monkeys were steeper for larger values of $\sum f$, that is, steeper for the larger sum for the 2 objects being compared (Fig. 4 *A* and *B*).

We quantified this phenomenon by estimating the just noticeable difference (JND), for each presented spatial frequency pair (22). We calculated, for each spatial frequency, the probability of choosing a second comparison frequency as a function of the unsigned difference between the standard stimulus and the comparison stimulus (*SI Appendix*, Fig. S3). We found that the JND increased proportionally to f (Fig. 4*C*), consistent with the Weber–Fechner law (23) and Steven's power law (24). The results could be described by a linear function: $JND(f) = 0.47f + 1.06$ for monkey M ($R^2 = 0.63$); $JND(f) = 0.37f + 0.77$ for monkey N ($R^2 = 0.95$).

There are a number of strategies that the monkeys could have used to compare the textures. One viable option could have been to use a consistent velocity when exploring both objects so that any variation in ICMS pulse rates between the objects could be explained by differences in spatial frequency alone. Further analysis revealed that this was not the case. Indeed, both monkeys used a distribution of speeds to sample the gratings (Fig. 5*A*) and could perform successful discriminations across the majority of their operating range (Fig. 5*B*)—only having difficulty when moving at very high speeds. Moreover, for the vast majority of trials, the average speeds used to scan the 2 objects differed, even within the same trial. Monkey M scanned the 2 objects with the same speed (speed difference < 1 cm/s) on fewer than 3% of trials. This effect cannot be explained by trial outcome (wrong trials: 2.41%, correct trials: 2.82%; *SI Appendix*, Fig. S4). Monkey N used the same scanning speed for each object on 3.85% of trials (3.95% of the wrong trials, 3.81% of the correct trials).

This variability in arm movements was sufficiently large that, in some cases, the ordinality of the spatial frequency of the textures was different from the ordinality of the ICMS pulse rates. An example of one of these apparently paradoxical trials is given in Fig. 5*C*. For this trial, the frequency of the right target ($f_R = 3.5$ ridges/cm) was higher than the left ($f_L = 2.5$ ridges/cm), but the actual average ICMS pulse rate delivered for the left target was higher than for the right (left: 200.2 Hz versus right: 103.1 Hz). This occurred because a faster avatar speed was used to explore the left target as compared to the right. Despite this, the monkey was able to accurately choose the target with the higher spatial frequency in this example.

We found many of these apparently paradoxical trials ($n = 1{,}231$, 12% of all trials) for monkey N. The majority of these cases corresponded with "difficult" frequency pairs, that is, comparisons with high $f_R + f_L$ (*SI Appendix*, Fig. S5). Monkey N's success rate was significantly above chance for these trials ($n = 1{,}231$, 56.1%, $P = 1.41 \times 10^{-5}$, 2-tailed binomial test; Fig. 5*D*). There were fewer of these trials for monkey M ($n = 329$, 6% of all trials). For these trials, monkey M's performance did not reach significance (52.03%, $P = 0.44$, 2-tailed binomial test).

BMBI with Active Texture Discrimination. Finally, we validated our stimulation paradigm in a closed-loop BMBI with monkey M. For this task, the monkey was allowed to move its arms, but the joystick was disconnected; instead the avatar arm—and task performance—was controlled via the decoding of 90 simultaneously

Downloaded at Palestinian Territory, occupied on November 29, 2021

www.manaraa.com

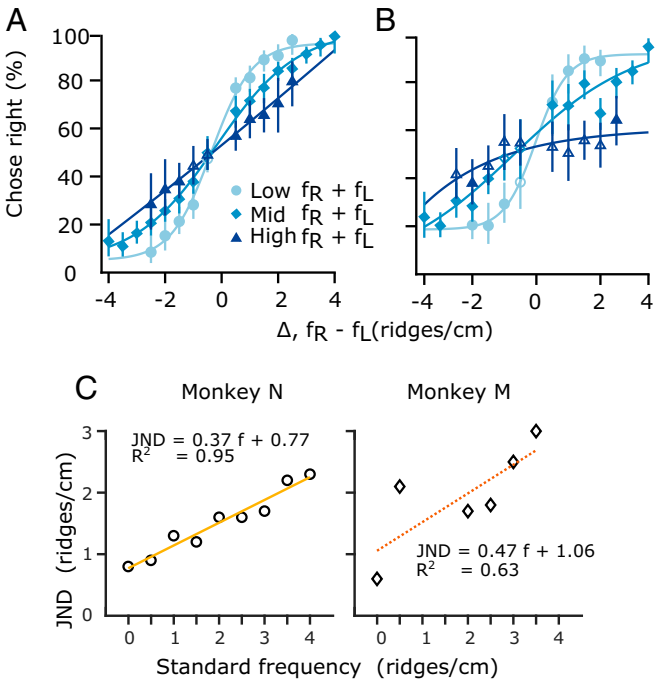

Fig. 4. Psychometrics analysis of artificial texture discrimination. (*A* and *B*) Discrimination of spatial gratings obeys Weber's scaling for monkey N (*A*) and monkey M (*B*). Each point represents the percentage of trials for which the monkey chose the right-most object, parameterized by the difference in spatial frequencies for a pair of objects (Δf, $f_R - f_L$) and the sum of the spatial frequencies ($f_R + f_L$) for low (less than 2.5 ridges/cm, circles), mid (between 2.5 and 5 ridges/cm, diamonds), and high (greater than 5 ridges/cm, triangles) sums. Filled symbols indicate discrimination significantly different from chance ($P < 0.05$, 2-sided binomial test). Error bars indicate 95% confidence intervals. Curves are the sigmoid lines of best fit. (*C*) JNDs for monkey M (diamonds) and N (circles), as a function of the standard frequency (detail of JND calculation for each standard frequency is shown on *SI Appendix*, Fig. S3; for monkey M JNDs for $f = 1$ and $f = 1.5$ were undefined). (*Inset*) Linear fits, the corresponding function and R^2 for each graph.

recorded right-hemisphere M1 neurons (Fig. 6*A*). We found that monkey M was able to control the avatar arm to explore the objects with minimal movement of its physical hand as can be seen in the examples shown in Fig. 6*B*. Moreover, when the hand did move, it made smaller movements with lower velocities than the simultaneous movements of the cursor during BMI trials ($n = 63$ trials; Fig. 6*C*), but the monkey could still control the cursor using cortical activity alone (Movie S2). The monkey retained the ability to accurately discriminate between the targets using the BMI; consistent with the non-BMI task, the monkey was significantly above chance in discriminating targets with Low $\sum f$ ($f_L + f_R < 2.5$ ridges/cm, 76%, $P = 0.02$, one-sided binomial test) but did not reach significance for medium ($f_L + f_R > 2.5$–5 ridges/cm, 65%, $P = 0.09$) or high $\sum f$ ($f_L + f_R > 5$ ridges/cm, 40%, $P = 0.21$; Fig. 6*D*).

Discussion

We have demonstrated an encoding strategy for texture representation using ICMS pulses in somatosensory cortex. Using this approach, 2 animals demonstrated discrimination of texture coarseness using active tactile exploration. Importantly, for this encoding, small variations of arm velocity changed stimulation frequency; the interpretation of the texture, therefore, may have employed a dynamic integration of ICMS stimulation information with arm proprioception feedback or corollary discharge of motor and sensory cortical regions (25). The apparently paradoxical trials provide evidence for these possibilities: Access to the movement command or proprioceptive feedback about the movement is necessary to disambiguate the exafference of the texture from the reafference due to movement.

We observed that both monkeys were better at discriminating textures when the overall spatial frequencies were small, consistent with the Weber–Fechner law (26), a phenomenon reported for numerous sensory modalities (27), including touch (28). Interestingly, this law was previously reported not to hold for the task of discriminating ICMS amplitude in primates (29) and humans (13). Our task, in contrast, required discriminating ICMS pulse rates, but, as it also used active exploration, we cannot rule out the possibility that some aspect of the effect is due to the motor act itself.

Our tactile encoding scheme was effective for a single channel of independent tactile information—mimicking a single mechanoreceptor localized in the fingertip. This encoding scheme most closely resembles the rapidly adapting (RA) afferents of cutaneous somatic sensation (30): Each pulse of ICMS was triggered by the intersection of the active zone of the avatar fingertip with a ridge on one of the gratings. However, there may be advantages of modeling a more slowly adapting type-1 (SA1) encoding on some additional channels. We believe that our encoding will be naturally extendable to arrays of mechanosensors embedded in the "skin" of a prosthetic limb, with each sensor connected to a channel of microstimulation in sensory cortex. For example, each feature in an object's tactile microstructure could trigger a pulse train of ICMS that persists for some finite duration. This type of encoding may allow an intuitive representation of the persistence of object–actuator contact interactions or complex representation of natural textures (31). However, several open questions remain, such as the optimal timescale or distribution of timescales for adaptation and whether the degree of adaptation must be matched to the properties of the specific neurons being stimulated. Work in primates (6, 32) and rats (33) suggests that the plasticity of the brain will allow even a few channels of stimulation to become effective at providing a rich sensory experience, and complex spatiotemporal coding (34) with enough bandwidth to be clinically useful.

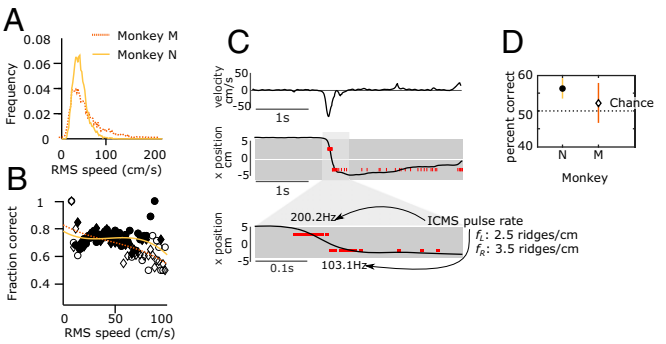

Fig. 5. Texture perception and arm movement. (*A*) Distribution of per-trial RMS exploration speeds. (*B*) Percentage of trials performed correctly as a function per-trial RMS speed for monkey M and monkey N. Curves are fourth-order polynomial fits. Filled symbols indicate discrimination significantly different from chance ($P < 0.05$, 2-sided binomial test). (*C*) An example of a paradoxical trial with monkey N. First 2 graphs indicate the x-component of the avatar velocity and the x-position. Gray rectangles indicate the position and horizontal dimension of the objects; their corresponding spatial frequencies were 2.5 and 3.5 ridges/cm, respectively. Vertical red lines indicate single pulses of ICMS. ICMS pulse rate were calculated for bursts of stimulation (a burst of stimulation was considered when the velocity magnitude was maintained above 10 [cm/s]). (*D*) Success rate of the paradoxical trials. The chance level is reported with a black dashed line. Error bars indicate 95% confidence intervals (2-sided binomial test).

Downloaded at Palestinian Territory, occupied on November 29, 2021
www.manaraa.com

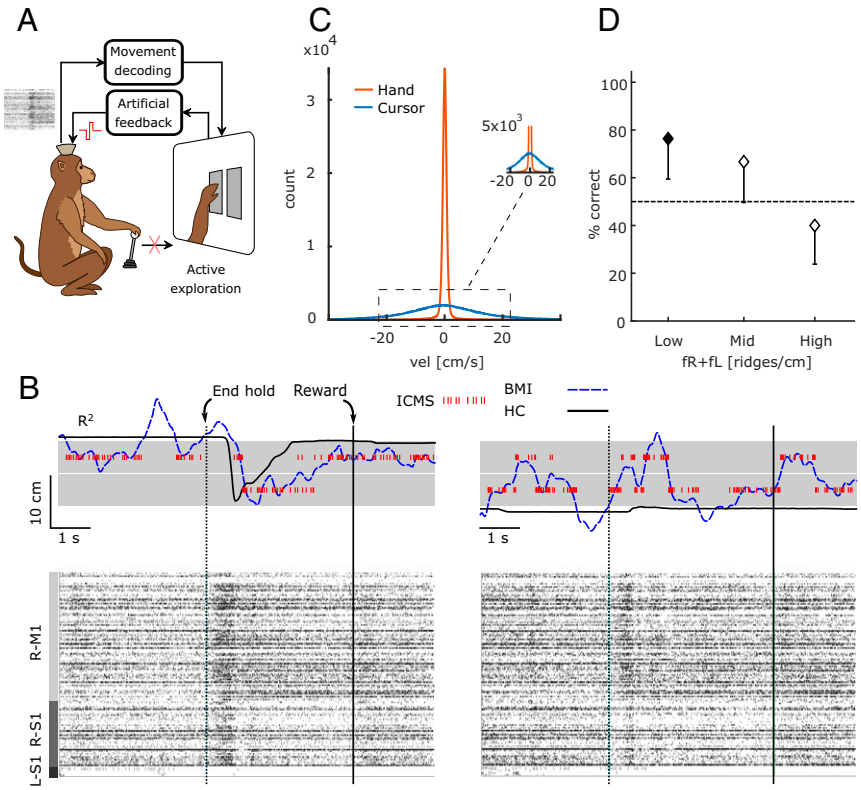

Fig. 6. BMI results. (*A*) Same experimental paradigm as in Fig. 1*A*, except that the control of the avatar arm was done via decoding of motor intention from monkey's motor cortex. The monkey has to hold the joystick during the task, was allowed to move the arm, but the joystick was disconnected. (*B*) Examples of 2 BMI trials and corresponding raster plots. Blue dashed lines report the x projection of the brain-controlled cursor (BMI) and solid black line the monkey's hand movement. ICMS pulses are shown with red vertical lines. Vertical dashed line is the end of the hold time (or onset of exploration), and solid line is the end of the trial and reward. Raster plots for the trials are grouped between 90 neurons in right hemisphere motor cortex area (R-M1), 47 neurons in right hemisphere sensory area (R-S1), and 5 neurons in the left hemisphere sensory area. (*C*) The distributions of velocity for the BMI controlled cursor (blue) distribution of the monkey's hand movements (orange). The hand movement was measured via the joystick movement (using the same gain as for hand control trials), and the trial was aborted if the monkey released the joystick handle. (*D*) Percentage success for BMI controlled trials, parameterized by the sum of the spatial frequencies ($f_R + f_L$) for low (less than 2.5 ridges/cm), mid (between 2.5 and 5 ridges/cm), and high (greater than 5 ridges/cm) sums. Error bars indicate 95% confidence intervals. Filled symbols are statistically different from chance ($P < 0.05$, one-sided binomial test).

In our experiment, monkey N was superior to monkey M in perceiving small differences of texture coarseness. While it is possible that this difference was due to a better comprehension of the task by monkey N, it could also reflect the fact that the stimulation region for monkey N was in the leg area while for monkey M it was in the receptive fields of the same arm used to control the joystick. Therefore, it is possible that interference between feedback from natural somatosensory pathways (hand touching the joystick, proprioception) and S1 ICMS feedback made task performance more difficult for monkey M. This indicates that further studies are necessary to determine, among other things, the best target in S1 for delivering ICMS that encodes tactile signals for future clinical neuroprosthesis. While delivering sensory feedback to an ethologically meaningful cortical area is likely beneficial for the subject to assimilate any limb prosthesis as a natural appendage (35–37), the use of different somatosensory regions in the cortex may facilitate the sensorymotor integration and tactile acuity. Therefore, we suggest that it may be necessary to deliver artificial sensory feedback to multiple cortical regions simultaneously to achieve the best performance of such limb prostheses.

One limitation of our experiment is that it cannot describe the nature of the monkeys' perception of the feedback or answer whether it mimics natural haptic sensations. Furthermore, we cannot determine whether the monkeys perceived the 2 cues as separate virtual objects or one single object with 2 material properties. However, our study clearly shows that monkeys can use our stimulation paradigm to detect differences in spatial frequency in a functionally useful manner. Importantly, the encoding paradigm is simple and can be easily integrated into existing neuroprosthetics. We note that both monkeys were able to learn to use the stimulation paradigm quickly, as both achieved discrimination accuracy significantly above chance from the very first session. This is in contrast with a purely associative mechanism, in which the monkeys would have learned to discriminate between different frequency pairs by a trial-and-error mechanism. Nevertheless, given the small number of subjects and the fact that both monkeys were familiar with ICMS from previous experiments, we cannot make strong claims about the "naturalness" of any percepts evoked by our stimulation paradigm.

Recently demonstrated clinical neuroprostheses have used modulation of stimulation amplitude (or equivalently, pulse width) to encode the perception of pressure, force, or position (8, 10, 38, 39). Our approach is complementary—stimulation pulse timing encodes coarse texture—and could be combined with the amplitude encoding approach to convey multimodal percepts of pressure and texture. However, some previous animal (40) and human (41) stimulation studies have provided indirect evidence that changes in pulse intensity (amplitude or pulse width) may be perceptually indistinguishable from changes in pulse rate. Further experiments will be necessary to conclusively determine if this is the case or if there is in fact an extra

Downloaded at Palestinian Territory, occupied on November 29, 2021

www.manaraa.com

degree of freedom that can be used to convey clinically relevant prosthetic sensations.

Finally, we demonstrated that our encoding strategy could be integrated within a closed-loop BMBI task. While the overall performance of the monkey for the BMBI task was lower than during arm control, the monkey was still able to discriminate the artificial textures. This, along with the simplicity of our ICMS encoding, suggests that this approach could be used to equip clinical upper-limb neuroprostheses with functional access to the tactile features of the natural world.

Materials and Methods

All animal procedures were performed in accordance with the National Research Council's Guide for the Care and Use of Laboratory Animals and were approved by the Duke University Institutional Animal Care and Use Committee.

Subjects and Implants. Two adult rhesus macaque monkeys (*Macaca mulatta*) participated in the experiments (monkeys M and N). Each monkey was implanted with four 96-microwire arrays constructed of insulated stainless steel 304. Each hemisphere received 2 arrays: one in the upper-limb representation area and one in the lower-limb representation area of sensorimotor cortex. These arrays covered both M1 and S1; only microwires implanted in S1 were used for delivering ICMS in the study. For the BMI task, we used recordings from the right hemisphere arm arrays as the monkey manipulated the joystick with the left arm.

Task. Each monkey sat in a primate chair, faced a computer screen, and grasped a joystick with their left hand. The joystick handle contained an optical sensor to indicate when the monkey released it. The monkeys were trained to manipulate the joystick to control the movements of a left upper-limb primate avatar on the screen (18, 42).

Each trial began with a circular target appearing in the center of the screen. The monkeys held an index finger of the avatar within this target for a delay randomly drawn from a uniform distribution parameterized from 200 to 2,000 ms. After this delay, the central target disappeared, and 2 rectangular object zones appeared on the screen. These appeared either both on the left side or both on the right side of the screen at a distance of 7 cm from the center. Both objects in the pair had the same width (6 cm). The spacing between the objects was 0.1 cm.

Vertical square-wave gratings were superimposed on each of the objects. These gratings, which were not visible to the monkeys, were aligned on the center of each object and were parameterized by spatial frequency, f. When the index finger of the avatar crossed a single ridge in a grating, a pulse of ICMS was delivered to a pair of electrodes implanted in S1 cortex. In this way, the pattern of ICMS delivered depended on the velocity of the avatar and the intrinsic spatial frequency of each grating.

Symmetric, biphasic, charge-balanced, cathode-leading ICMS pulses were delivered in a bipolar fashion across pairs of microwires. The channels selected had clear sensory receptive fields in the left forearm (monkey M: 2 pairs of microwires) or left lower limb (monkey N: 1 pair of microwires).

Monkeys received a reward for selecting the object from the pair with the higher spatial frequency, f, drawn from:

$$f \in \{0,0.5, 1.0, 1.5, 2.0, 2.5, 3.0, 3.5, 4.0\} \text{ ridges/cm},$$

with the constraint that both objects did not share the same f on a single trial. Monkey M did not discriminate the gratings as reliably and so was not presented any gratings with the highest spatial frequency, 4.0 ridges/cm. The monkeys indicated their choice by holding the avatar over one of the objects for the hold interval (2 s for the hand control and 1 s for the BMBI task). Selecting the object with the higher f triggered the delivery of a fruit juice reward; selecting the object with lower f ended the trial without reward.

The object locations—and the spatial frequencies associated with each—were randomly generated for each trial. However, we repeated the presentation of a frequency pair after an incorrect selection. These "correction trials" were used to keep the monkeys motivated and to prevent them from acquiring systematic biases. As the rewarded object was known to the monkeys for correction trials, we excluded these trials from all analyses.

The objects could be explored in any sequence. Moreover, objects could be reexplored and recompared multiple times in a trial. However, the avatar had to pass over both objects at least once per trial. Trials for which only a single object was explored were terminated without reward, even if the correct object was ultimately selected. Trials for which the monkey released the joystick handle at any time, selected the wrong object, made a selection without exploring both objects, or held the avatar outside of either of the objects for 10 s, resulted in the termination of a trial and penalty interval of 2 s for monkey M and 2.5 s for monkey N.

BMI Decoding. A 10th-order Unscented Kalman filter was used for BMI predictions, using methods we previously described (18, 43). The filter parameters were fit using the hand movements made while the task was performed using a joystick. The monkey was permitted to continue moving the joystick but was only rewarded for target selections made with the brain-controlled cursor.

ACKNOWLEDGMENTS. We thank D. Dimitrov for conducting the animal surgeries; J. Fruh for the design of the monkey avatar; and G. Lehew, J. Meloy, T. Phillips, L. Oliveira, Amol Yadav, and S. Halkiotis for technical support. This research was supported by the NIH Director's Pioneer Award DP1-OD006798 and by NIH's National Institute of Neurological Disorders and Stroke Award R01NS073952 (to M.A.L.N.). The content is solely the responsibility of the authors and does not necessarily represent the official views of the Office of the NIH Director or the NIH.

1. M. A. Lebedev, M. A. L. Nicolelis, Brain-machine interfaces: Past, present and future. *Trends Neurosci.* **29**, 536–546 (2006).
2. J. L. Collinger, R. A. Gaunt, A. B. Schwartz, Progress towards restoring upper limb movement and sensation through intracortical brain-computer interfaces. *Curr. Opin. Biomed. Eng.* **8**, 84–92 (2018).
3. B. S. Wilson *et al*., Better speech recognition with cochlear implants. *Nature* **352**, 236–238 (1991).
4. M. S. Humayun *et al*., Visual perception in a blind subject with a chronic microelectronic retinal prosthesis. *Vision Res.* **43**, 2573–2581 (2003).
5. R. A. Normann, E. M. Maynard, P. J. Rousche, D. J. Warren, A neural interface for a cortical vision prosthesis. *Vision Res.* **39**, 2577–2587 (1999).
6. N. A. Fitzsimmons, W. Drake, T. L. Hanson, M. A. Lebedev, M. A. Nicolelis, Primate reaching cued by multichannel spatiotemporal cortical microstimulation. *J. Neurosci.* **27**, 5593–5602 (2007).
7. R. Romo, A. Hernández, A. Zainos, E. Salinas, Somatosensory discrimination based on cortical microstimulation. *Nature* **392**, 387–390 (1998).
8. D. W. Tan *et al*., A neural interface provides long-term stable natural touch perception. *Sci. Transl. Med.* **6**, 257ra138 (2014).
9. D. J. Atkins, D. C. Y. Heard, W. H. Donovan, Epidemiologic overview of individuals with upper-limb loss and their reported research priorities. *J. Prosthet. Orthot.* **8**, 2–11 (1996).
10. S. Raspopovic *et al*., Restoring natural sensory feedback in real-time bidirectional hand prostheses. *Sci. Transl. Med.* **6**, 222ra19 (2014).
11. P. D. Marasco, A. E. Schultz, T. A. Kuiken, Sensory capacity of reinnervated skin after redirection of amputated upper limb nerves to the chest. *Brain* **132**, 1441–1448 (2009).
12. C. M. Oddo *et al*., Intraneural stimulation elicits discrimination of textural features by artificial fingertip in intact and amputee humans. *Elife* **5**, e09148 (2016).
13. S. N. Flesher *et al*., Intracortical microstimulation of human somatosensory cortex. *Sci. Transl. Med.* **8**, 361ra141 (2016).
14. E. Moberg, Criticism and study of methods for examining sensibility in the hand. *Neurology* **12**, 8–19 (2012).
15. J. R. Flanagan, A. M. Wing, Modulation of grip force with load force during point-to-point arm movements. *Exp. Brain Res.* **95**, 131–143 (1993).
16. R. S. Johansson, G. Westling, Roles of glabrous skin receptors and sensorimotor memory in automatic control of precision grip when lifting rougher or more slippery objects. *Exp. Brain Res.* **56**, 550–564 (1984).
17. R. S. Johansson, J. R. Flanagan, Coding and use of tactile signals from the fingertips in object manipulation tasks. *Nat. Rev. Neurosci.* **10**, 345–359 (2009).
18. J. E. O'Doherty *et al*., Active tactile exploration using a brain-machine-brain interface. *Nature* **479**, 228–231 (2011).
19. S. J. Lederman, R. L. Klatzky, Hand movements: A window into haptic object recognition. *Cogn. Psychol.* **19**, 342–368 (1987).
20. J. E. O'Doherty, M. A. Lebedev, Z. Li, M. A. L. Nicolelis, Virtual active touch using randomly patterned intracortical microstimulation. *IEEE Trans. Neural Syst. Rehabil. Eng.* **20**, 85–93 (2012).
21. L. E. Medina, M. A. Lebedev, J. E. O'Doherty, M. A. L. Nicolelis, Stochastic facilitation of artificial tactile sensation in primates. *J. Neurosci.* **32**, 14271–14275 (2012).
22. R. Ulrich, D. Vorberg, Estimating the difference limen in 2AFC tasks: Pitfalls and improved estimators. *Atten. Percept. Psychophys.* **71**, 1219–1227 (2009).
23. A. Gescheider, *Psychophysics: The Fundamentals* (Lawrence Erlbaum Assoc., Mahwah, NJ, ed. 3, 1997).
24. S. S. Stevens, On the psychophysical law. *Psychol. Rev.* **64**, 153–181 (1957).
25. T. B. Crapse, M. A. Sommer, Corollary discharge across the animal kingdom. *Nat. Rev. Neurosci.* **9**, 587–600 (2008).
26. G. Ekman, Weber's Law and related functions. *J. Psychol.* **47**, 343–352 (1959).
27. S. Dehaene, The neural basis of the Weber-Fechner law: A logarithmic mental number line. *Trends Cogn. Sci.* **7**, 145–147 (2003).
28. E. H. E. H. Weber, *Weber on the Tactile Senses* (E.H. Weber on the Tactile Senses, 2018).

Downloaded at Palestinian Territory, occupied on November 29, 2021
www.manaraa.com

29. S. Kim *et al*., Behavioral assessment of sensitivity to intracortical microstimulation of primate somatosensory cortex. *Proc. Natl. Acad. Sci. U.S.A.* **112**, 15202–15207 (2015).
30. S. J. Bolanowski, G. A. Gescheider, R. T. Verrillo, C. M. Checkosky, Four channels mediate the mechanical aspects of touch. *J. Acoust. Soc. Am.* **84**, 1680–1694 (1988).
31. J. D. Lieber, S. J. Bensmaia, High-dimensional representation of texture in somatosensory cortex of primates. *Proc. Natl. Acad. Sci. U.S.A.* **116**, 3268–3277 (2019).
32. M. C. Dadarlat, J. E. O. Doherty, P. N. Sabes, A learning-based approach to artificial sensory feedback leads to optimal integration. *Nat. Neurosci.* **18**, 138–144 (2015).
33. E. E. Thomson, R. Carra, M. A. L. Nicolelis, Perceiving invisible light through a somatosensory cortical prosthesis. *Nat. Commun.* **4**, 1482 (2013).
34. K. Hartmann *et al*., Embedding a panoramic representation of infrared light in the adult rat somatosensory cortex through a sensory neuroprosthesis. *J. Neurosci.* **36**, 2406–2424 (2016).
35. G. Rognini *et al*., Multisensory bionic limb to achieve prosthesis embodiment and reduce distorted phantom limb perceptions. *J. Neurol. Neurosurg. Psychiatry* **90**, 833–836 (2018).
36. S. Shokur *et al*., Expanding the primate body schema in sensorimotor cortex by virtual touches of an avatar. *Proc. Natl. Acad. Sci. U.S.A.* **110**, 15121–15126 (2013).
37. K. L. Collins *et al*., Ownership of an artificial limb induced by electrical brain stimulation. *Proc. Natl. Acad. Sci. U.S.A.* **114**, 166–171 (2017).
38. E. D'Anna *et al*., A closed-loop hand prosthesis with simultaneous intraneural tactile and position feedback. *Sci. Robot.* **4**, eaau8892 (2019).
39. E. L. Graczyk *et al*., The neural basis of perceived intensity in natural and artificial touch. *Sci. Transl. Med.* **8**, 362ra142 (2016).
40. G. Y. Fridman, H. T. Blair, A. P. Blaisdell, J. W. Judy, Perceived intensity of somatosensory cortical electrical stimulation. *Exp. Brain Res.* **203**, 499–515 (2010).
41. L. A. Johnson *et al*., Direct electrical stimulation of the somatosensory cortex in humans using electrocorticography electrodes: A qualitative and quantitative report. *J. Neural Eng.* **10**, 036021 (2013).
42. P. J. Ifft, S. Shokur, Z. Li, M. A. Lebedev, M. A. L. Nicolelis, A brain-machine interface enables bimanual arm movements in monkeys. *Sci. Transl. Med.* **5**, 210ra154 (2013).
43. Z. Li *et al*., Unscented Kalman filter for brain-machine interfaces. *PLoS One* **4**, e6243 (2009).

Downloaded at Palestinian Territory, occupied on November 29, 2021

www.manaraa.com